Free-fermion approach to the commensurate-incommensurate transition in a model of Si/W(110)

J. Amar and J. D. Gunton
Physics Department, Temple University, Philadelphia, Pennsylvania 19122
(Received 13 May 1985)

The existence and stability of the incommensurate phase in a lattice-gas model of Si adsorbed on W(110) is studied using domain-wall arguments and the free-fermion approximation. The incommensurate phase observed in a previous Monte Carlo study is shown to be stable above both the (5×1) and (6×1) phases in agreement with the general prediction for $(p\times1)$ phases. The commensurate-incommensurate transition lines from the ordered (5×1) and (6×1) phases to the incommensurate phase are calculated using the low-temperature free-fermion approximation. The results are shown to be in good qualitative agreement with results from previous Monte Carlo simulations.

I. INTRODUCTION

In a previous paper,[1] the phase diagram for the system consisting of Si on W(110) based on a lattice-gas model (using pair interactions obtained from field-ion microscopy[2]) on a centered-rectangular lattice (see Fig. 1) was studied—using both Monte Carlo simulation techniques and transfer-matrix scaling. In this study, ordered (5×1) and (6×1) phases were predicted in addition to the $p(2\times1)$ phase which had been observed (at low coverage) in the field-ion-microscopy studies. In addition, an incommensurate phase was found to exist in the region above the (5×1) and (6×1) phases and possibly in the region between them at low temperature (see Fig. 5). In this paper we explain the existence of this incommensurate phase as being due to *walls* between ordered regions. These walls (and their corresponding kinks) are the low-lying excitations of the system for values of the field h near the degeneracy field h^* where the (5×1) and (6×1) phases become degenerate. The stability of the incommensurate phase with respect to dislocations is also studied and good qualitative agreement for the commensurate-incommensurate transition lines at low temperature is found. We note that in what follows, we sketch only the basic outline of the calculation, which was performed following the approach of Villain and Bak in Ref. 3. For further details, the reader is referred to Refs. 3 and 4.

II. MODEL

The Hamiltonian for our lattice-gas model includes six pair interactions (see Fig. 1) and can be written (in Ising-spin language) as

$$H=\tfrac{1}{4}\sum_{\left[\substack{i,j\\ i<j}\right]} J(\mathbf{r}_{ij})s_i s_j - h\sum_i s_i \ , \tag{1}$$

where the s_i are Ising spins ($s_i=\pm1$), h is a magnetic field, and the pair interactions are $J_1=0$, $J_2=38$, $J_3=-50$, $J_4=47.5$, $J_5=10$, and $J_6=-5$ meV. This Hamiltonian consists of a strong attractive (ferromagnetic) interaction in the J_3 direction combined with strong repulsive interactions in the J_4 and J_2 directions. The ground states thus consist essentially of ferromagnetic chains running in the J_3 direction, which are repelled by the J_2 and J_4 interactions and which are weakly attracted via the J_6 interaction. It is the competition between the repulsive J_2 and J_4 interactions and the attractive J_6 interaction which is responsible for the incommensurate phase in our model.

For the field in the range $0<h<h^*$, where $h^*=24.7$ is the value of the field at which both the (6×1) and (5×1) ground states become degenerate,[1] the ground state is the (6×1) phase shown in Fig. 2(a). For $h^*<h<73.05$, the ground state is the (5×1) phase. This may be viewed [see Figs. 2(b) and 2(d)] as a (6×1) phase with a domain-wall density of $\frac{1}{5}$, where a wall essentially consists of a region in which the chains which characterize the (6×1) state move one step closer together in the b direction. Thus, the energy of the (5×1) phase can be written as the energy of the (6×1) phase plus the extra contribution due to the walls. The wall energy consists of two parts: (a) the extra energy due to pair interactions at the walls and (b) the decrease in magnetic field energy due to the extra spin densi-

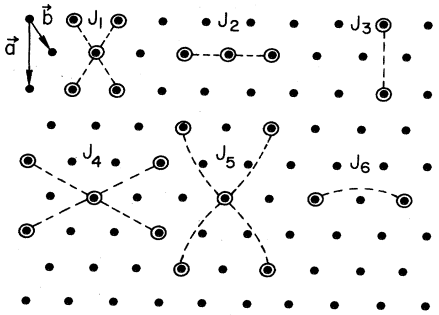

FIG. 1. Diagram showing first- through sixth-nearest-neighbor interactions. The vectors **a** and **b** indicate the primitive lattice vectors of the centered-rectangular lattice.

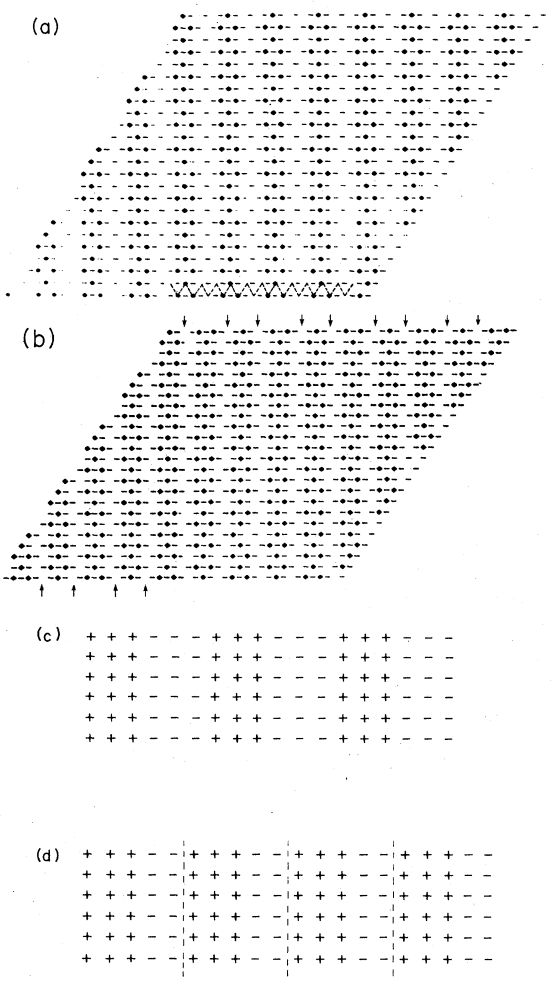

FIG. 2. (a) Picture of a 24×24 portion of the ordered (6×1) phase (coverage equals 0.5) taken from Monte Carlo simulations. Solid diamonds indicate Si adatoms while the spaces indicate vacant adatom sites. (Dashes serve merely to separate sites.) (b) Ordered (5×1) phase (coverage equals 0.4), as seen in Monte Carlo simulations. Arrows indicate walls. (c) The (6×1) phase (mapped onto a rectangular lattice) showing uniaxial ordering. (d) The (5×1) phase (mapped onto a rectangular lattice). Dashed lines represent walls (wall density equals $\frac{1}{5}$).

ty at the walls [see Fig. 2(d)]. At the degeneracy field h^*, the extra pair-interaction energy of a wall is exactly canceled out by the extra magnetic field energy contribution. Thus, at h^*, the energy of a wall is zero and the (6×1) and (5×1) phases are degenerate at zero temperature. Formally, one may write

$$E_{6\times1}=E_{5\times1}+\tfrac{1}{5}(h^*-h)=E_{5\times1}+(\tfrac{1}{5})E_w\ , \tag{2}$$

where E_w is the wall energy per unit length in the b direction. Thus, one obtains

$$E_w=h^*-h\ . \tag{3}$$

For sufficiently low temperature ($k_BT\ll J_3$) and h near h^* ($h<h^*$, $E_w\ll k_BT$) the dominant excitation of the (6×1) phase will consist of walls produced by thermal excitation. Similarly, for $h>h^*$ the (5×1) state (wall density equal to $\frac{1}{5}$) will be favored energetically but due to thermal fluctuations the equilibrium wall density will be *less* than $\frac{1}{5}$. Therefore, the equilibrium state of the system will consist of regions of the pure (6×1) state separated by domain walls with a wall density q between 0 and $\frac{1}{5}$. Thus, the system will be incommensurate in the b direction—a uniaxial incommensurate state. (In the limit q goes to zero, the incommensurability or deviation of the wave vector q_i characterizing the periodicity in the **b** direction from its commensurate value q_c is given by $q_i-q_c=2\pi q/6$.) At low temperature the free energy of the system may be simply regarded as the free energy of a system of domain walls, with the wandering entropy of the walls (due to kinks) providing the stabilizing force for the incommensurate phase. Thus, the equilibrium wall density q is directly determined by a competition between the energy of formation of a wall (E_w) and the wandering entropy of walls due to kinks.

In Figs. 3(a) and 3(b) we show the two types of kinks ($K1$ and $K2$) which are the lowest-energy excitations of a wall. Configurations of walls with kinks like those shown were observed in the Monte Carlo studies in the incommensurate phase. We note that, as far as the field-energy contribution of a kink is concerned, one cannot, strictly speaking, calculate the energy of a single kink—since, de-

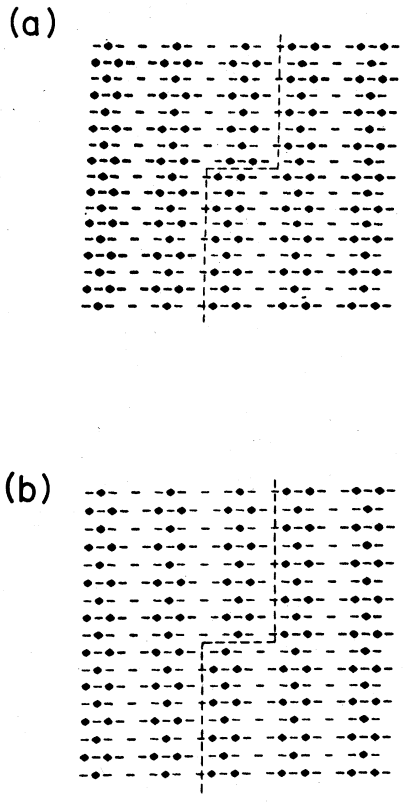

FIG. 3. (a) Kink of type $K1$ shown on centered rectangular lattice. $E_{K1}=J_4-J_3-h=97.5$ meV$-h$. (b) Kink of type $K2$ shown on centered rectangular lattice. $E_{K2}=2J_3+h=50$ meV$+h$.

pending on the boundary conditions there will be an additional contribution to the energy of a kink at the boundary.[4] However, one can calculate the energy of a pair of kinks, since for a pair of kinks (such as a left and a right kink) the boundary contribution no longer exists. The energy of a single kink is then taken to be the energy of such a pair divided by 2. Figures 4(a) and 4(b) illustrate the energy calculations for a pair of kinks of types $K1$ and $K2$. The results are

$$E_{K1}=J_4-J_3-h\ , \tag{4}$$

$$E_{K2}=-J_3+h\ . \tag{5}$$

We note that the energy of these kinks ($K1$ and $K2$)— in contrast to previous studies[3,5,6]— is a function of the field h. The field dependence is perhaps more clearly seen when the kinks are mapped onto a rectangular lattice as in Figs. 4(c) and 4(d). In what follows, we shall assume that the dominant excitation for a given value of the field h is the kink with lowest energy—which we shall denote as E_k. We note that near the degeneracy field h^* ($h^*=24.7$ meV), which is where we expect our low-temperature approximation to be applicable, $K1$ has energy $E_{K1}=72.8$ meV and $K2$ has energy $E_{K2}=74.7$ meV. Thus, both types of kinks have approximately the same energy at h^*. Therefore, our system at low temperature (for a given value of the field h) can be approximately mapped into a system of walls and kinks with a given kink energy E_k.

III. FREE-FERMION CALCULATION

In order to perform the calculation of the free energy of our system of walls and kinks we first map the system from a centered-rectangular lattice to a "rectangular" one where a path in a zigzag horizontal direction [see Fig. 2(a)] becomes the x coordinate while the y coordinate corresponds to the vertical direction. In this new coordinate system the existence of a wall and of the two types of kinks can be more clearly seen [see Figs. 2(c), 2(d), 4(c), and 4(d)]. We now perform a mapping from the "rectangular" coordinate system with coordinates x and y to a new system with coordinates ξ and y using the following transformation:

$$\xi=[(x+p)/6]\ . \tag{6}$$

Here, p refers to the number of the first wall to the left of the point (x,y) in the "rectangular system", and [ ] means to use the integer part. This transformation maps our original rectangular system with dimensions N_y and N_x (for a system with ν walls) to one with dimensions N_y and $(N_x+\nu)/6$. In this new coordinate system, the minimum distance between walls and the kink-step distance become equal to one (in units of the lattice constant). This transformation enables one not to have to worry about wall crossings since they are now taken care of automatically using the free-fermion formalism.

In the limit of low temperature (no dislocations), the partition function corresponding to a system with ν walls may now be written as

$$Z(\nu)=E_0^{N_y}\exp(-\beta\nu E_w)C(\nu)\ , \tag{7}$$

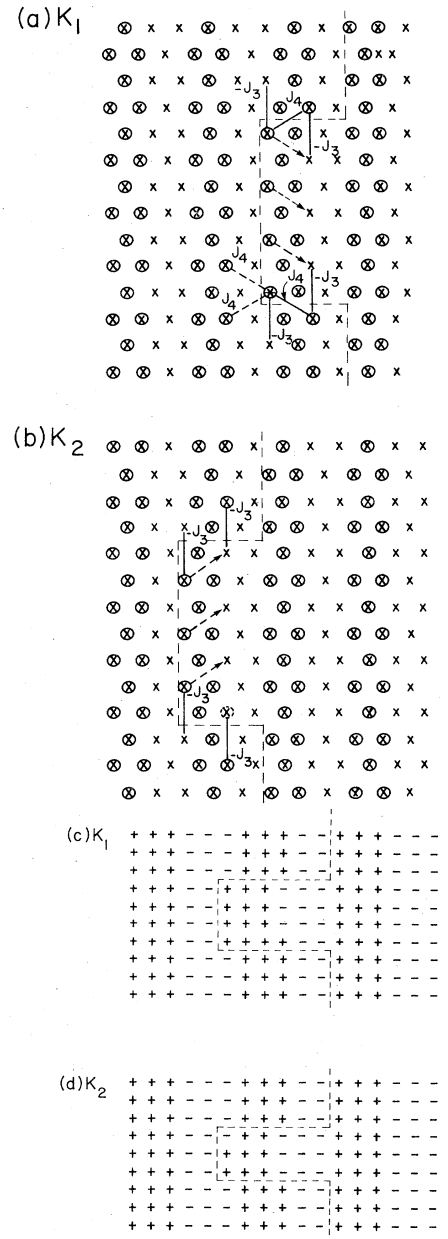

FIG. 4. (a) Diagram showing calculation of energy for pair of kinks of type $K1$. Thin-dashed line indicates wall. Extra bonds are indicated by solid lines ($-J_3$ and J_4) and thick-dashed lines (J_4). Dashed arrows indicate motion of occupied sites to remove pair of kinks (straight wall). Note that there is one *extra* occupied site (denoted by $*$) thus creating an energy contribution of $-2h$ to the kink-pair energy. Counting the contributions to the kink energy due to the extra bonds (times 2), and remembering the factor of $\frac{1}{4}$ in the definition of the pair interactions [Eq. (1)] we get the result in Eq. (4). (b) Diagram showing calculation of energy of pair of kinks of type $K2$. Energy due to extra bonds is again shown by labeled heavy bonds. Arrows indicate motion of occupied sites to remove kinks. Dashed circle indicates energy contribution ($+2h$) due to extra *empty* (spin down) site. Including the contributions to the kink energy due to the extra bonds, we get the result in Eq. (5). (c) Pair of kinks $K1$ [same as (a)] mapped onto rectangular lattice. (d) Pair of kinks $K2$ [same as (b)] mapped onto rectangular lattice.

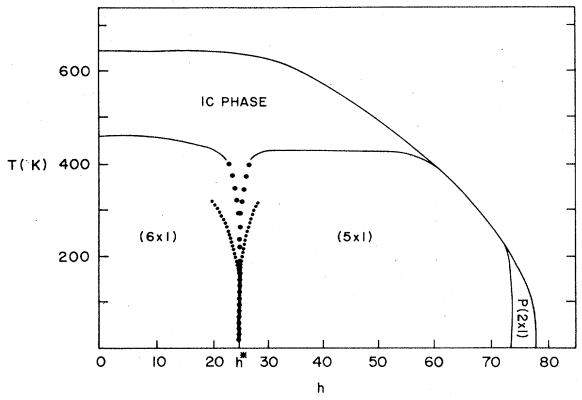

FIG. 5. Phase diagram for our model of Si/W(110). The solid line indicates Monte Carlo simulation results taken from Ref. 1. (Large dots are an extrapolation of Monte Carlo data.) The small-dotted line indicates free-fermion results obtained from Eqs. (11) and (12). IC denotes the incommensurate phase.

where E_w is given by Eq. (3) above, $C(\nu)$ reflects boundary effects that can be neglected in the thermodynamic limit, and E_0 is the largest eigenvalue of the transfer matrix Θ which serves to create (destroy) walls (i.e., introduce kinks) as one travels in the y (time) direction. Using the free-fermion formalism, in which walls are represented as fermions so that no two walls may cross, the transfer matrix Θ may be written as

$$\Theta=\exp\left[\gamma\left[\sum_{\xi} c^{\dagger}(\xi)c(\xi+1)+c^{\dagger}(\xi+1)c(\xi)\right]\right], \tag{8}$$

where the fermion operator $c^{\dagger}(\xi)$ $\{c(\xi)\}$ creates (destroys) a wall at position ξ and $\gamma=\exp(-\beta E_k)$ is the Boltzmann factor for the kink of lowest energy E_k. Evaluating E_0 by diagonalizing Θ one gets the following expression for the partition function as a function of the number of walls ν:

$$Z(\nu)=\exp\left[N_y\left\{\frac{\gamma(N_x+\nu)}{3\pi}\sin\left[\frac{6\pi\nu}{N_x+\nu}\right]-\nu\beta(h-h^*)\right\}\right]. \tag{9}$$

Minimizing this expression as a function of the density of walls q ($q=\nu/N_x$) is equivalent to minimizing the free energy and gives

$$0=(1/6\pi)\sin\{6q\pi/(1+q)\}+\{1/(1+q)\}\cos\{6q\pi/(1+q)\}-A\ , \tag{10}$$

where $A=\beta(h^*-h)/2\gamma$. Equation (10) has nontrivial solutions for A in the range $-\frac{5}{6}<A<1$, which corresponds to q in the range $\frac{1}{5}>q>0$. Setting $q=0$ ($A=1$) in Eq. (10) we get an equation for the commensurate-incommensurate transition from the (6×1) phase to the incommensurate phase:

$$\beta(h^*-h)=2\exp(-\beta E_k)\quad(h<h^*)\ . \tag{11}$$

Setting $q=\frac{1}{5}$ ($A=-\frac{5}{6}$) we get the equation for the commensurate-incommensurate transition from the (5×1) phase:

$$\beta(h^*-h)=-(\tfrac{5}{3})\exp(-\beta E_k)\quad(h>h^*)\ . \tag{12}$$

The solution of these two equations is plotted in Fig. 5, together with our Monte Carlo results for the (5×1)-incommensurate and (6×1)-incommensurate transitions. The steepness of the (5×1) and (6×1) commensurate-incommensurate transition lines at low temperature explains why it was difficult in the Monte Carlo simulations to see clearly the incommensurate phase in between the two ordered phases at low T. We note that this treatment ignores the possibility of higher-energy excitations, such as double kinks, and thus our results are expected to overestimate the transition temperature at low temperatures. However, as pointed out in Ref. 1, strong finite-size effects (pinning of the incommensurate phase) in the Monte Carlo study also lead to an overestimation of the transition temperature (see solid line in Fig. 5). Thus, it is not surprising that, in Fig. 5, the Monte Carlo results are actually somewhat above our results obtained from Eqs. (11) and (12) (in the low-temperature region where the free-fermion approximation is expected to be valid).[7] In addition, the possible effects of dislocations on the stability of the incommensurate phase have been ignored. In the following section we consider the effects of dislocations on the stability of the incommensurate phase near the commensurate phase in the same manner as was done by Villain and Bak.[3]

IV. STABILITY OF INCOMMENSURATE PHASE

Following the work of Villain and Bak on the axial next-nearest-neighbor Ising model,[3] it can be shown that in the long-wavelength limit (ignoring dislocations), the free energy for the incommensurate phase can be expressed in terms of a Hamiltonian which is equivalent to that for the XY model. Kosterlitz and Thouless[8] have shown that the incommensurate or floating phase characterized by this Hamiltonian is unstable with respect to the formation of vortices (i.e., dislocations) if the correlation-function exponent η is greater than $\frac{1}{4}$. Thus, if the value of η near the commensurate-incommensurate transition lines for the (5×1) and (6×1) phases is less than $\frac{1}{4}$, we expect the incommensurate phase to be stable above both commensurate phases. General arguments for such models as the p-state chiral clock model[9] and the sine-Gordon model[10] (which are expected to exhibit transitions in the same universality class as those for $(p\times1)$ adsorbed phases[11]) give a value of $\eta=2/p^2$. Thus η is less than $\frac{1}{4}$ for $p=5,6$, and therefore we would expect the incommensurate phase to be stable above the (5×1) and (6×1) phases in the low-temperature approximation. Using the free-fermion approximation,[3] we have calculated the value of the exponent η at low temperature as a function of the wall density q. Our result is

$$\eta=\tfrac{1}{18}(1+q)^2\ . \tag{13}$$

Substituting the value of q appropriate for the (6×1)-incommensurate transition ($q=0$) we see that this gives a

value of η in agreement with the general form (for $p=6$). Similarly, substituting the value of $q=\frac{1}{5}$ [near the (5×1)-incommensurate transition] gives the value $\eta=\frac{2}{25}$, again in agreement with the general formula. Thus, we conclude that the incommensurate phase is indeed stable above the (5×1) and (6×1) phases. Hence we have shown both the existence and stability of the incommensurate phase which was previously predicted from our previous Monte Carlo study. We note that since the incommensurate phase is stable above both the (5×1) and (6×1) phases, the incommensurate-disorder transition does not extend to zero temperature as in Refs. 3 and 4. Thus, a low-temperature or perturbative estimate of the incommensurate-disorder transition due to dislocations as performed by Villain and Bak is not expected to be valid. We note that, at the temperatures at which dislocations are expected to appear, the structure of the chains becomes more disordered and more complicated kink structures (seen in the Monte Carlo study) are expected to appear.

ACKNOWLEDGMENTS

This work was supported by National Science Foundation Grant No. DMR-8312958 and by U. S. Office of Naval Research Grant No. N00014-83-K-0382.

[1]J. Amar, S. Katz, and J. D. Gunton, Surf. Sci. **155**, 667 (1985).
[2]R. Casanova and T. T. Tsong, Thin Solid Films **93**, 41 (1982).
[3]J. Villain and P. Bak, J. Phys. (Paris) **42**, 657 (1981).
[4]J. Amar, Ph.D. thesis, Temple University, 1985.
[5]E. Domany and B. Schaub, Phys. Rev. B **29**, 4095 (1984).
[6]P. Rujan, W. Selke, and G. V. Uimin, Z. Phys. B **53**, 221 (1983).
[7]Substituting a value of 0.1 for q [the pinned value of the wall density found in the Monte Carlo (MC) study, see Ref. 1] in Eq. 10 gives a "transition line" for $h>h^*$ which fits the MC data almost perfectly at low temperature (up to approximately 400 K)—thus confirming the expected finite-size dependence of the MC study.
[8]J. M. Kosterlitz and D. J. Thouless, J. Phys. C **6**, 1181 (1973).
[9]S. Ostlund, Phys. Rev. B **24**, 398 (1981).
[10]H. J. Schulz, Phys. Rev. B **28**, 2746 (1983).
[11]D. A. Huse and M. E. Fisher, Phys. Rev. B **29**, 239 (1984).